

## Optimization Design Methodology of Miniaturized Five-Band Antenna for RFID, GSM, and WiMAX Applications

Ayia A. S. A. Jabar and Dhirgham K. Naji\*

**Abstract**—This paper presents a novel design methodology for the design and optimization of a miniaturized multiband microstrip patch antenna (MPA) for wireless communication systems. Two design steps are used to do that. In the first step, an initial antenna is designed by a trial and error approach to operate nearly in the desired frequency bands, but the level of impedance matching ( $s_{11} < -10$  dB) for one or more bands is unsatisfactory, or some bands are uncovered by the antenna. The second design step is used after that to achieve optimized antenna by applying an optimization algorithm to effectively fine-tune the impedance matching of the initial designed antenna to closely satisfy all the desired frequency bands. As an illustrative example, the proposed optimization methodology is used for designing a miniaturized multiband MPA suitable for operating at five different frequency bands, 915 MHz (RFID band), 1850 MHz (GSM band), (ISM — Industrial, Scientific, Medical), 2.45 and 5.8 GHz, and 3.5 GHz (WiMAX band). The proposed MPA used here is composed of two patch structures printed on both sides of an FR4 substrate occupying an overall size of just  $28 \times 28$  mm<sup>2</sup>. The final optimized antenna is fabricated, and its simulated and measured results are coinciding with each other validating the design principle. Moreover, simulation antenna performance parameters, surface current distribution, realized peak gain, and efficiency besides the radiation patterns at the desired frequency bands are obtained using CST MWS.

### 1. INTRODUCTION

In recent years, much interest has been paid to the study and design of multiband antennas for use in mobile communication systems covering all the desired frequency bands needed by international standard. Due to the limited space for these applications, designing a multiband antenna having satisfactory performance is a challenging task. Miniaturized antennas with multiband characteristic for mobile wireless applications, such as internet of things [1–4], wireless sensor networks [5], wearable devices [6, 7], RFID portable devices [8–12], and implantable biomedical systems [13, 14], have become urgent requirements. Over the past decade, various methods and optimization techniques have been introduced for multiband or wideband antenna design. Some of the most commonly used techniques for solving different electromagnetic problems particularly antenna design are a genetic algorithm (GA) [15–21], simulated annealing (SA) [22, 23], invasive weed optimization (IWO) [24–26], and particle swarm optimization (PSO) [27–33]. The proposed antennas presented in these papers clarify the advantages of PSO algorithm such as easy implementation and suitability for use in the design of those optimized antennas including single- and multi-objective optimization problems compared with other aforementioned techniques GA, SA, and IWO.

Antenna optimization is greatly dependent on an efficient objective function that leads to an optimizer for getting desirable solution in the visible region. Generally in the literature, two

---

*Received 29 January 2019, Accepted 14 March 2019, Scheduled 27 March 2019*

\* Corresponding author: Dhirgham Kamal Naji (dhrgham.kamal@gmail.com).

The authors are with the Department of Electronic and Communications Engineering, College of Engineering, Al-Nahrain University, Baghdad, Iraq.

conventional objective functions ( $F$ ) to be minimized, namely,  $F_1 = \max(|S_{11}(f)|)$  [22, 27, 28, 33] and  $F_2 = \text{sum}(|S_{11}(f)|_{\text{dB}})$  [15, 16, 20, 21, 23], where  $f$  is the sample frequency ranging from  $f_{\min}$  to  $f_{\max}$ , are used for designing a multiband antenna. The objective functions  $F_1$  and  $F_2$  are minimized for getting an improvement in  $|S_{11}(f)|$  and the area under  $|S_{11}(f)|_{\text{dB}}$ , respectively for the all sample frequencies resulting in an antenna having wide or multiband characteristic [34].

In general, two well-known methods are recently available for solving multi-objective optimization problems: (1) Pareto dominance (PD) [30, 35, 36] and (2) conventional weighted aggregation (CWA) [15, 16, 20–29]. In a PD method, all competing single-objective functions for the optimization problem can be simultaneously dealt with by the designers through deriving complete Pareto front (PF) that exposes the compromise between those objectives resulting in miscellaneous representations of the optimal solutions. Whatever, although PD methods are suitable for solving multi-objective optimization problems particularly for antenna design, for many problems, large number of iterations and optimization calculations are required. A complete PF must be obtained, especially in problems that contain many design targets and antenna geometrical parameters. On the other hand, in a CWA approach, a number of discrete weighting coefficients of single-objective functions are added to constitute the objective function that allows all single-objective functions to be minimized simultaneously. This method is simple to be implemented for antenna optimization problems by properly finding the convenience aggregation of weighting coefficients for the assortment of single-objective functions. Also, the CWA approach is especially easy in optimization problems when the desired objectives are related or use same physical units [37] such as the multi-objective function for the designed antenna presented in this work.

In this paper, a novel optimization objective function is proposed for designing multiband antenna under the constraint of miniaturized size. This objective function for the first time deals with both the lower and higher frequencies that belong to the all desired frequency bands. In this work, the PSO kernel implemented in MATLAB and finite integration technique (FIT) offered by CST Microwave Studio (MWS) are operated in parallel to evaluate the objective function. As an illustrative example, a five-band antenna is optimized to cover the desired bands allocated for sub-6 GHz applications: 915 MHz and 2.45/5.8 GHz for RFID, 1850 MHz for GSM, 2.4/5.8 GHz for WLAN, and 3.5 GHz for WiMAX. The designed antenna is verified experimentally.

## 2. PROPOSED OPTIMIZATION METHODOLOGY

To find the best solution that treats a certain problem, optimization technique is used. The optimization of geometric parameters for any application-based microwave/RF device becomes very crucial since the device is necessary to exhibit a particular desired response. For optimizing the microwave designs, Evolutionary Algorithms (EAs) involve GA, PSO, SA, and IWO which have been used as very reliable methods. These EA algorithms can be used to optimize many parameters simultaneously, and they overcome the local minima problems in most of the cases. Compared to other EAs techniques such as GA, SA, and IWO, the PSO algorithm is much easier to understand and implement, and requires the least mathematical preprocessing. Therefore, it is well adopted here to be used in the design optimization of the proposed antennas.

The procedure of PSO optimization resembling the social behavior of a swarm of bees while searching for the region with most flowers. It is based on a population of particles that fly in space with velocity dynamically adjusted according to its own flying experience and the flying experience of the best among the swarm. Each potential solution in the PSO algorithm is represented as a particle with a position vector of  $\mathbf{x} = (x_1, x_2, \dots, x_N)$  and velocity  $\mathbf{v} = (v_1, v_2, \dots, v_N)$  in an  $N$ -dimensional optimization. An associated value for each particle, at each time step, is evaluated according to an objective function which is critically configured with a consideration of the search objective. In the PSO, it is firstly generating a population of  $N_p$  particles at random to search a broad population of possible solution in the entire search space. Generally, using a defined objective function, for all particles the objective values are evaluated, and the global best ( $x^{\text{best}}$ ) and personal best ( $x_i^{\text{best}}$ ) are calculated which are used in producing the new position  $x_{i+1}$  and new velocity  $v_{i+1}$  for each particle after each iteration  $i + 1$ . Thus, at iteration  $i + 1$ ,  $v_{i+1}$  and  $x_{i+1}$  for each particle are updated by:

$$v_{i+1} = \omega v_i + 2\eta_1 \left( x_i^{\text{best}} - x_i \right) + 2\eta_2 \left( x^{\text{best}} - x_i \right) \quad (1)$$

$$x_{i+1} = x_i + v_{i+1} \tag{2}$$

In Eq. (1), the time varying parameter  $\omega$ , which is called inertia factor, decreases with iteration number from a maximum value at the first iteration and goes to a minimum at the last iteration. Two statistically independent random variables  $\eta_1$  and  $\eta_2$ , both uniformly distributed in the interval  $[0, 1]$ , are introduced to stochastically vary the relative pull of the personal and global best particles. The designs are optimized PSO integrated with CST Microwave Studio.

Mathematically, the nonlinear global optimization problem to be solved in this work is defined as:

Find the set  $\mathbf{x} = (x_1, x_2, \dots, x_N)$  of  $N_g$  geometrical antenna parameters that will optimize the function

$$\text{Minimize} \quad F(\mathbf{x}) \tag{3a}$$

$$\text{subject to} \quad h(\mathbf{x}) = 0, \quad g(\mathbf{x}) \leq 0 \tag{3b}$$

$$\text{and the constraints:} \quad x_i^l \leq x_i \leq x_i^u \quad i = 1, 2, \dots, N_g,$$

where  $F(\mathbf{x})$  described in Eq. (3) is the objective function,  $h(\mathbf{x})$  the equality constraint,  $g(\mathbf{x})$  the inequality constraint, and  $\mathbf{x}$  the vector of design variables. Also,  $x_i^l$  and  $x_i^u$  are the lower and upper bounds on the  $N$  design variables, respectively.

The goal for using PSO considered here was aimed to achieve optimized antenna by tuning CST simulated frequency bands to the counterpart desired bands by altering the initial designed antenna geometrical parameters within allowed prescribed ranges. A suitable optimization model to satisfy this aim is:

$$\begin{aligned} \text{Minimize} \quad F(\mathbf{x}) &= -\frac{1}{2} [F_1 + F_2 + \dots + F_k], \\ &= -\frac{1}{2} \sum_{i=1}^K F_i, \quad i = 1, 2, 3, \dots, K \end{aligned} \tag{4a}$$

$$\text{Subject to} \quad A_{\text{opt}} = A_{\text{ref}} \tag{4b}$$

$$\text{and the constraints:} \quad x_i^l \leq x_i \leq x_i^u \quad i = 1, 2, \dots, N_g,$$

In this model,  $A_{\text{opt}}$  and  $A_{\text{ref}}$  represent area of the optimized antenna and the reference antenna, respectively.

At the  $j$ th band ( $1 \leq j \leq K$ ):

$$F_j = W_{Lj} E_{Lj} + W_{Hj} E_{Hj} \tag{5}$$

where

$$E_{Lj} = U(-f_{Lj} + f_{dLj}^{\text{max}}) + U(f_{Lj} - f_{dLj}^{\text{min}}) \tag{6a}$$

$$E_{Hj} = U(-f_{Hj} + f_{dHj}^{\text{max}}) + U(f_{Hj} - f_{dHj}^{\text{min}}) \tag{6b}$$

and

$$W_{Lj} = \frac{f_{dLj}^{\text{min}}}{f_{Lj}} \tag{7a}$$

$$W_{Hj} = \frac{f_{Hj}}{f_{dHj}^{\text{max}}} \tag{7b}$$

$$f_{Lj} = f \left| \begin{array}{l} S_{11} \text{ at } f_{Lj} = -10 \text{ dB} \\ \frac{dS_{11}}{df} = -1 \end{array} \right. \tag{8a}$$

$$f_{Hj} = f \left| \begin{array}{l} S_{11} \text{ at } f_{Hj} = -10 \text{ dB} \\ \frac{dS_{11}}{df} = +1 \end{array} \right. \tag{8b}$$

$$S_{11 \text{ at } f_{Lj}} = 20 \log \left| \frac{Z_{\text{in at } f_{Lj}} - Z_o}{Z_{\text{in at } f_{Lj}} + Z_o} \right| \text{ (dB)} \quad (9a)$$

$$S_{11 \text{ at } f_{Hj}} = 20 \log \left| \frac{Z_{\text{in at } f_{Hj}} - Z_o}{Z_{\text{in at } f_{Hj}} + Z_o} \right| \text{ (dB)} \quad (9b)$$

In the objective function above, Eq. (6),  $U$  refers to the unit step function while  $E_{Lj}$  and  $E_{Hj}$  denote, respectively, the error of the  $j$ th  $-10$ -dB  $S_{11}$  impedance bandwidth ( $BW_j = f_{Hj} - f_{Lj}$ ) where  $f_{Lj}$  and  $f_{Hj}$  denote, respectively, the  $j$ th lower and higher frequencies. In Eq. (9),  $S_{11 \text{ at } f_{Lj}}$ ,  $S_{11 \text{ at } f_{Hj}}$  and  $Z_{\text{in at } f_{Lj}}$ ,  $Z_{\text{in at } f_{Hj}}$  refer, respectively, to the return loss and the input impedance of the antenna at  $f_{Lj}$ ,  $f_{Hj}$ , and  $Z_o$  is the characteristic impedance ( $Z_o = 50 \Omega$ ). The symbols  $W_{Lj}$  and  $W_{Hj}$  represent the weighting coefficients corresponding to the  $j$ th error functions  $E_{Lj}$  and  $E_{Hj}$ , respectively, and  $K$  refers to the number of desired frequency bands. The '+' sign in  $F(\mathbf{x})$  is a logic "AND" addition, and the values of  $E_{Lj}$  and  $E_{Hj}$  are either logic '1' or logic '0'. Thus, for each calculated  $j$ th frequency band  $BW_j$  to be greater than the  $j$ th desired band ( $BW_{dj} = f_{dHj} - f_{dLj}$ ),  $E_{Lj}$  and  $E_{Hj}$  are equal to one, and otherwise they are equal to zero, where  $f_{dHj}$  and  $f_{dLj}$  are the  $j$ th desired high and low frequencies, respectively. On the other hand, the ranges of weighting coefficients  $W_{Lj}$  and  $W_{Hj}$  are, respectively,  $(f_{dLj}^{\min}/f_{dLj}^{\max}) \leq W_{Lj} \leq 1$  and  $(f_{dHj}^{\min}/f_{dHj}^{\max}) \leq W_{Hj} \leq 1$ . To easily understand the concepts of Eqs. (4)–(9), see the following two comments.

- a) The error of  $j$ th lower frequency  $E_{Lj} = U(-f_{Lj} + f_{dLj}^{\max}) + U(f_{Lj} - f_{dLj}^{\min})$  where the first term is

$$U(-f_{Lj} + f_{dLj}^{\max}) = \begin{cases} 1, & f_{Lj} \leq f_{dLj}^{\max} \\ 0, & f_{Lj} > f_{dLj}^{\max} \end{cases}, \quad (10a)$$

and the second term is

$$U(f_{Lj} - f_{dLj}^{\min}) = \begin{cases} 1, & f_{Lj} \geq f_{dLj}^{\min} \\ 0, & f_{Lj} < f_{dLj}^{\min} \end{cases}. \quad (10b)$$

Thus, if both terms of  $E_{Lj}$  are equal to 1, then  $E_{Lj} = 2$ , which means that  $f_{dLj}^{\min} \leq f_{Lj} \leq f_{dLj}^{\max}$ , or the  $j$ th lower frequency  $f_{Lj}$  is satisfied to range between the minimum and maximum values of the  $j$ th desired lower frequency  $f_{dLj}^{\min}$  and  $f_{dLj}^{\max}$ , respectively.

- b) In the same manner, the error of the  $j$ th higher frequency  $E_{Hj} = U(-f_{Hj} + f_{dHj}^{\max}) + U(f_{Hj} - f_{dHj}^{\min})$ , where its first term is

$$U(-f_{Hj} + f_{dHj}^{\max}) = \begin{cases} 1, & f_{Hj} \leq f_{dHj}^{\max} \\ 0, & f_{Hj} > f_{dHj}^{\max} \end{cases}, \quad (11a)$$

and the second term is

$$U(f_{Hj} - f_{dHj}^{\min}) = \begin{cases} 1, & f_{Hj} \geq f_{dHj}^{\min} \\ 0, & f_{Hj} < f_{dHj}^{\min} \end{cases} \quad (11b)$$

Thus, if both terms of  $E_{Hj}$  are equal to 1, then  $E_{Hj} = 2$ , which means that  $f_{dHj}^{\min} \leq f_{Hj} \leq f_{dHj}^{\max}$ , or the  $j$ th higher frequency  $f_{Hj}$  is satisfied to range between the minimum and maximum values of the  $j$ th desired higher frequency  $f_{dHj}^{\min}$  and  $f_{dHj}^{\max}$ , respectively. As a result, if all the bands ( $i = 1, 2, \dots, K$ ) are satisfied,  $F(\mathbf{x})$  will be at a minimum value given by:

$$F(\mathbf{x}) = \begin{cases} -K, & \text{if } W_{Li} = W_{Hi} = 1 \\ -K \sum_{i=1}^K (W_{Li} + W_{Hi}), & \text{if } W_{Li} \neq 1 \text{ and } W_{Hi} \neq 1 \end{cases}, \quad i = 1, 2, \dots, K \quad (12)$$

A block diagram related to the proposed optimization model, Eqs. (4)–(9), is shown in Figure 1, which describes these equations in descending manner. Six blocks are required to efficiently calculate the objective function defined in Eq. (4). These main blocks, as described in Figure 1 in detail, are summarized in the following:

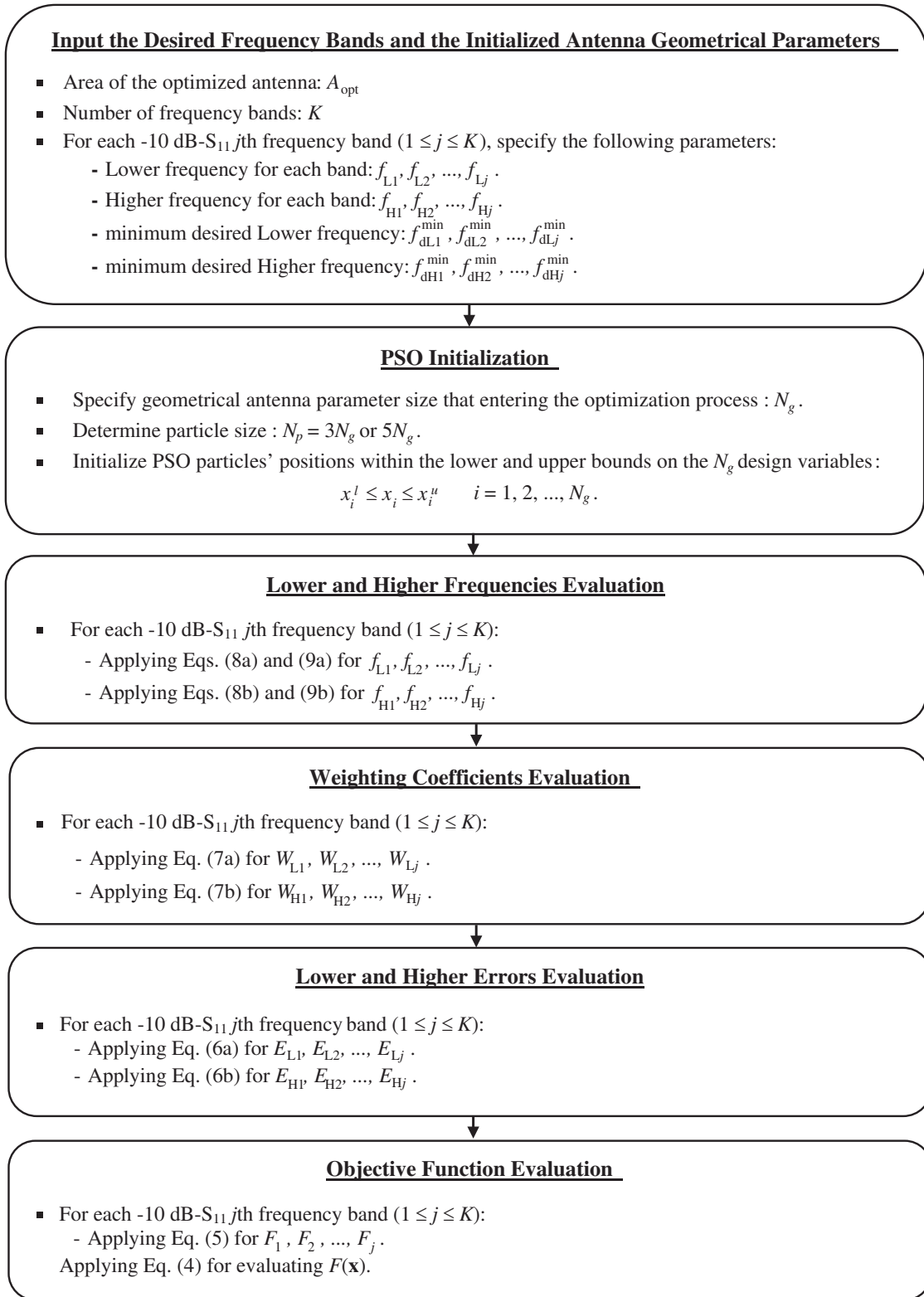


**Figure 1.** The main six blocks that related to the proposed optimization model of Eqs. (4)–(9).

- First Block (Input the Desired Frequency Bands and the Initialized Antenna Geometrical Parameters):* The optimization model begins by using a trial and error approach for the proposed antenna, which has an overall size of  $A_{\text{ref}}$  and initialized geometrical parameters for operating nearly throughout some desired frequency bands. In this step, the number of frequency bands  $K$ , the area of the optimized antenna  $A_{\text{opt}}$ , and for each  $-10$  dB- $S_{11}$   $j$ th frequency band ( $1 \leq j \leq K$ ): the lower frequencies  $f_{L1}, f_{L2}, \dots, f_{Lj}$ , higher frequencies  $f_{H1}, f_{H2}, \dots, f_{Hj}$ , minimum desired Lower frequency  $f_{dL1}^{\min}, f_{dL2}^{\min}, \dots, f_{dLj}^{\min}$ , and minimum desired higher frequency:  $f_{dH1}^{\min}, f_{dH2}^{\min}, \dots, f_{dHj}^{\min}$  are specified.
- Second Block (PSO Initialization):* In PSO initialization phase, it is required to specify the number of geometrical antenna parameters entering the optimization process ( $N_g$ ) and the particle size  $N_p$  ( $= 3N_g$  or  $5N_g$ ), in addition to PSO particles' positions allowed to cover the space search,  $x_i^l \leq x_i \leq x_i^u$  for  $i = 1, 2, \dots, N_g$ .
- Third Block (Lower and Higher Frequencies Evaluation):* The goal of the proposed model is for covering all the  $j$ th  $-10$  dB- $S_{11}$  frequency bands ( $1 \leq j \leq K$ ) by the optimized antenna. Eqs. (8a) and (9a) are used for evaluating  $f_{L1}, f_{L2}, \dots, f_{Lj}$ , whereas Eqs. (8b) and (9b) are employed for calculating  $f_{H1}, f_{H2}, \dots, f_{Hj}$ .
- Fourth Block (Weighting Coefficients Evaluation):* In this step, for each  $j$ th  $-10$  dB- $S_{11}$  frequency band ( $1 \leq j \leq K$ ), the lower and higher weighting coefficients,  $W_{L1}, W_{L2}, \dots, W_{Lj}$ , and  $W_{H1}, W_{H2}, \dots, W_{Hj}$ , are calculated by applying Eqs. (7a) and (7b), respectively.
- Fifth Block (Lower and Higher Errors Evaluation):* In this step, for each  $j$ th  $-10$  dB- $S_{11}$  frequency band ( $1 \leq j \leq K$ ), the lower and higher errors,  $E_{L1}, E_{L2}, \dots, E_{Lj}$ , and  $E_{H1}, E_{H2}, \dots, E_{Hj}$ , are calculated by applying Eqs. (6a) and (6b), respectively.
- Sixth Block (Objective Function Evaluation):* This is the final step in the optimization model that evaluates the multi-objective function  $F(\mathbf{x})$  by applying Eq. (4) with summing the all single-objective functions  $F_1, F_2, \dots, F_j$ .

### 3. ANTENNA DESIGN VIA OPTIMIZATION METHODOLOGY

The objective function discussed in the previous section is applied here to design, as an illustrative example, an optimized antenna having multiband characteristic under the constraint of miniaturized size. The concept of two well-known techniques, fractal and spiral geometries because of their main characteristics, multiband and miniaturization, is adopted for designing MPAs using the aforementioned optimization methodology. In this work, the antenna is optimized using two softwares running in parallel, PSO technique implemented under MATLAB environment, while the electromagnetic (EM) part of the objective function was offered by CST Microwave Studio software package. At each iteration of the PSO algorithm, initial designed antenna geometrical parameters are updated to CST MWS to extract the EM simulated result, antenna return loss  $S_{11}$ . Then,  $S_{11}$  result is mapped again in MATLAB for evaluating the objective function (multiband impedance matching criterion) by the PSO algorithm. This optimization process as shown in Figure 2 is still for running until enough number of iterations is reached, and consequently an optimized antenna with satisfied performance is obtained. Generally, the following two main steps are performed:

#### 1) First Design Step

In this step, a trial and error approach is used for designing an initialized antenna having both multiband behavior and miniature structure suitable for using in wireless communication systems. This initialized antenna with a size of  $A_{\text{ref}}$  can be nearly operated within some of the desired frequency bands with unsatisfactory level of impedance matching, and the other bands may not be covered by the antenna. Therefore, it is a challenging task by antenna designers to achieve antennas satisfying all the desired bands simultaneously by using a trial and error method. Thus, it is necessarily needed to use an optimization methodology for fine-tuning the antenna geometrical parameters performing the aforementioned challenging task for designing such antennas. Hence, an initialized antenna obtained in this step is used in step 2 for initializing  $N_p$ -particles of the PSO algorithm.

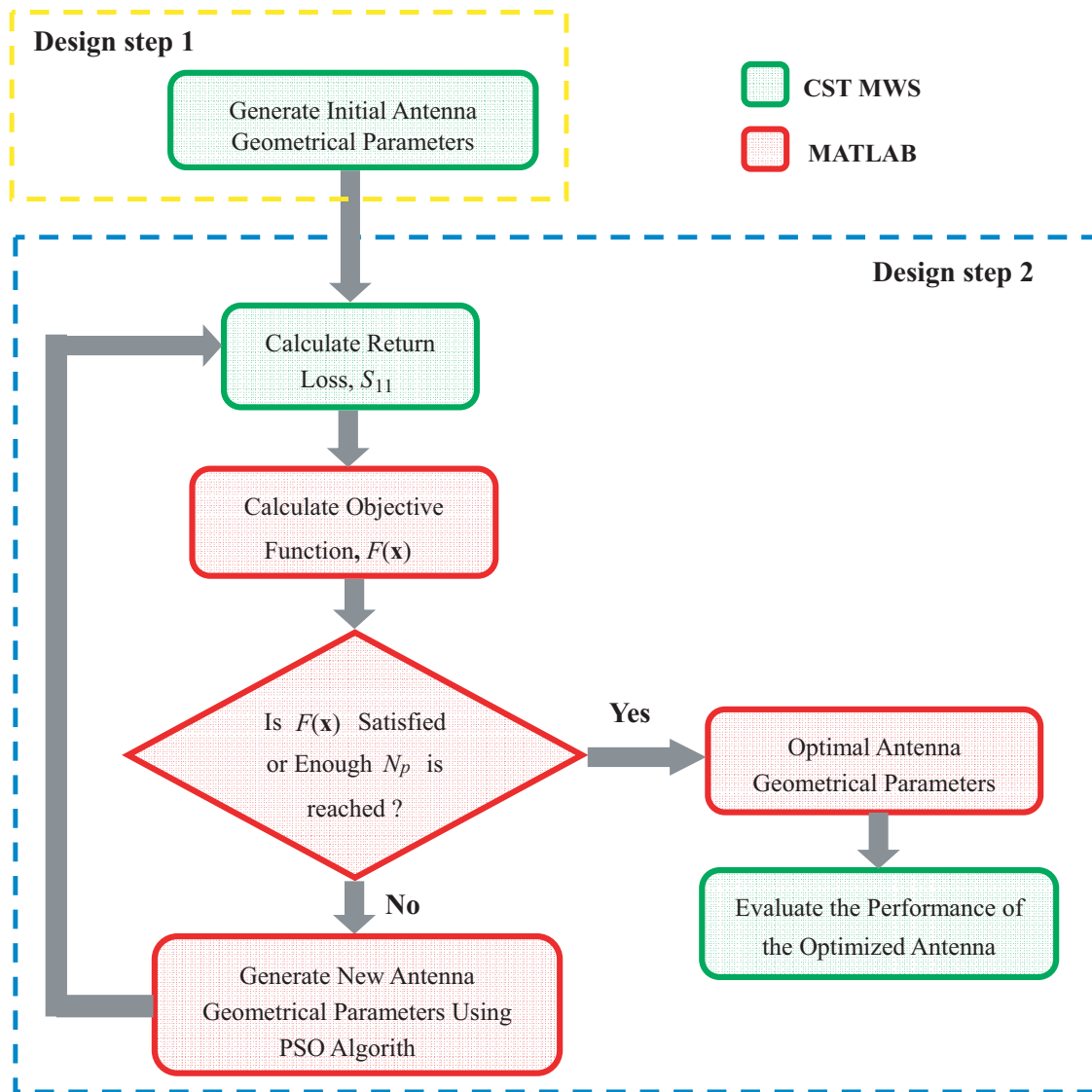


**Figure 2.** Data flow for designing both the initialized and optimized antennas. The initial designed antenna geometrical parameters are taken from the optimized antenna.

**2) Second Design Step**

In this step, the procedure presented in Section 2 is applied to the initialized antenna. This procedure yields an optimized antenna size of  $A_{opt} = A_{ref}$  and operating over the desired frequency bands by applying Eqs. (4)–(9) for describing the objective function.

**3.1. Initial Design of Fractal- and Spiral-Shaped Patch Antenna**

To validate the effectiveness of the optimization methodology in antenna design, a new proposed antenna structure is chosen as an illustrative example to optimize it by applying the two design steps discussed earlier for simultaneously covering the desired different five frequency bands. These five bands include: 915-MHz RFID band (860–960 MHz), 1850-MHz GSM band (1800–1900 MHz), 2.45-GHz RFID/WLAN band (2.40–2.50 GHz), 3.5-GHz 5G band (3.4–3.6 GHz), and 5.8-GHz RFID/WLAN band (5.725–5.875 GHz). The initialized designed antenna is proposed to attain these bands by using fractal- and spiral-shaped structures in the front and back sides of the FR4 substrate, respectively. Then an optimized antenna will be obtained through applying optimization methodology, described in

Eqs. (4)–(9), to the initialized antenna structure aiming to cover the appropriate bands. The following sections present in details the description and investigation of the procedure for designing and analyzing the proposed antenna structure that achieves the aforementioned frequency bands under the constraint of miniaturized size.

Figures 3(a)–(d) show the simulation models 3D and 2D besides the front and back sides, respectively of the proposed initial designed antenna, and the front and back sides of the manufactured optimized antenna are depicted, respectively, in Figures 3(e)–(f). The antenna includes two structures printed on both sides of an FR4 substrate with overall dimensions ( $L_{sub} \times W_{sub}$ ) of (28 mm  $\times$  28 mm) with thickness  $h_{sub}$  1.6 mm, relative permittivity  $\epsilon_r = 4.3$ , and loss tangent 0.02. A second-order Minkowski fractal-shaped patch strip is printed on the front side of the FR4 substrate, and on its back side a spiral-shaped loop structure is printed.

The fractal-shaped strip patch antenna length and width are, respectively,  $L_p = 12$  mm and  $W_p = 14$  mm, and thickness  $t_f = 0.5$  mm. The spiral width and length are, respectively,  $L_{sp} = 22$  mm and  $W_{sp} = 22$  mm, and its thickness  $t_s = 0.5$  mm. The spacing between strips  $d = 5$  mm. A 50- $\Omega$  SMA is connected to the bottom side of coplanar waveguide (CPW)-feed, with length ( $L_f = 9$  mm) and width ( $W_f = 2$  mm), and another side of the feed line is connected to the fractal patch strip for signal transmission. A linearly tapered ground plane, having a width ( $W_1 = 12.75$  mm) and length ( $L_g = 5$  mm), is printed at the gap ( $g = 0.25$  mm) from the CPW-feed line for widening impedance bandwidth.

### 3.2. Design Procedure of Initialized Antenna

The structural evolution of the proposed initialized designed antenna, which comprises seven design structures, is shown in Figure 4, and the optimized values of those antenna parameters are listed in Table 1. Figure 5 plots the CST simulated return loss ( $S_{11}$ ) results of the antennas. The design and analysis of these seven structures besides their  $S_{11}$  results will be extensively investigated in the next subsections.

**Table 1.** The final dimensions of the designed antennas.

parameter	Value (mm)						
	Ant0	Ant1	Ant2	Ant3	Ant4	Ant5	Ant6
$L_{sub}$	28.0	28.0	28.0	28.0	28.0	28.0	28.0
$W_{sub}$	28.0	28.0	28.0	28.0	28.0	28.0	28.0
$h_{sub}$	1.5	1.5	1.5	1.5	1.5	1.5	1.5
$L_p$	12.0	12.0	12.0	12.0	12.0	12.0	12.0
$W_p$	15.0	14.0	14.0	14.0	14.0	14.0	14.0
$L_f$	9.0	9.0	9.0	9.0	9.0	9.0	9.0
$W_f$	2.0	2.0	2.0	2.0	2.0	2.0	2.0
$L_s$	4.0	NA	NA	NA	NA	NA	NA
$W_s$	0.5	NA	NA	NA	NA	NA	NA
$g$	NA	0.25	0.25	0.25	0.25	0.25	0.25
$L_g$	NA	5.0	5.0	5.0	5.0	5.0	5.0
$W_1$	NA	NA	12.75	12.75	12.75	12.75	12.75
$t_1$	NA	NA	0.5	0.5	0.5	0.5	0.5
$L_{sp}$	NA	NA	NA	NA	22.0	22.0	22.0
$W_{sp}$	NA	NA	NA	NA	22.0	22.0	22.0
$W_2$	NA	NA	NA	NA	5.0	5.0	3.5
$t_2$	NA	NA	NA	NA	0.5	0.5	0.5
$L_1$	NA	NA	NA	NA	NA	NA	0.5

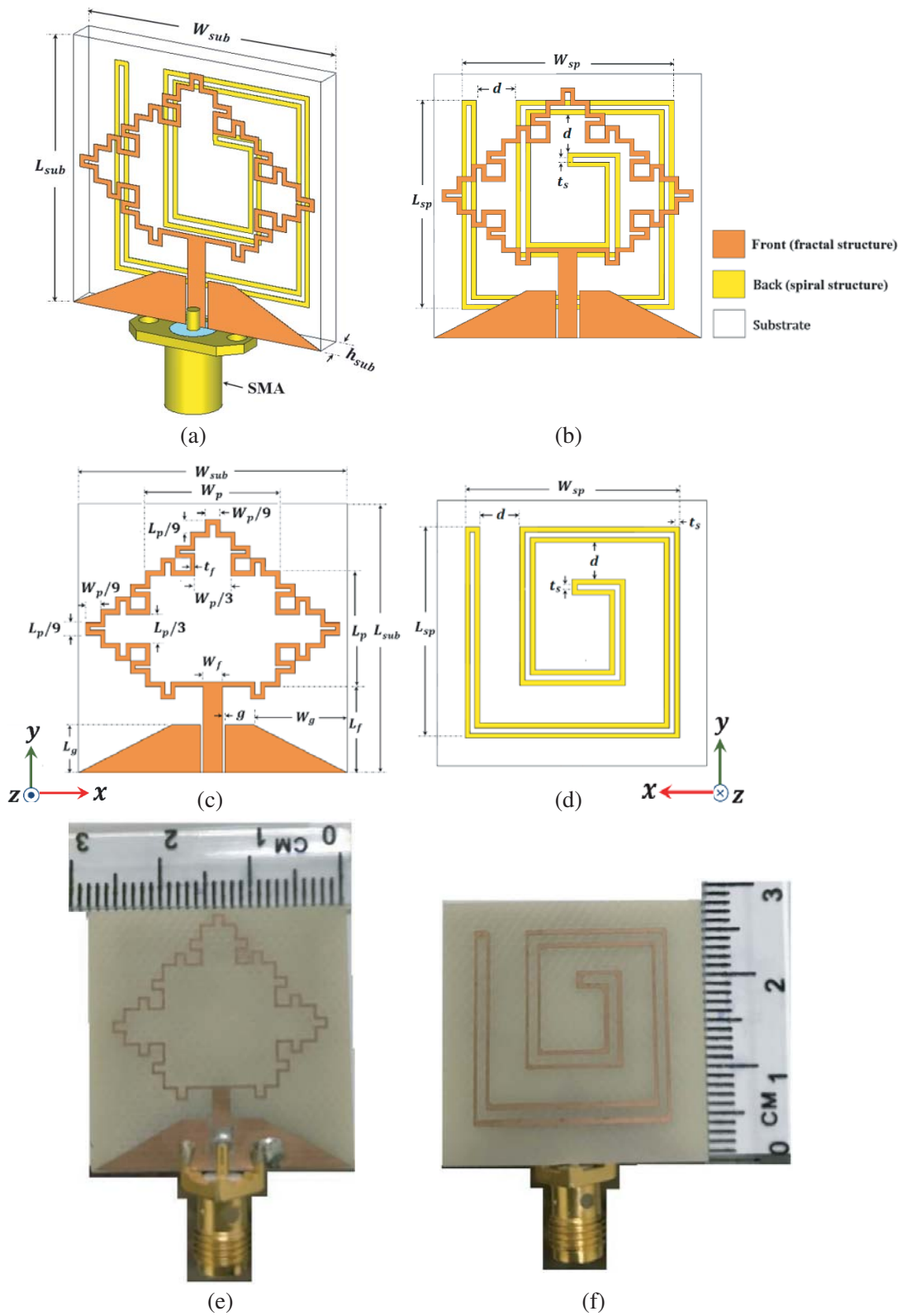


Figure 3. Geometry of the proposed designed antenna.

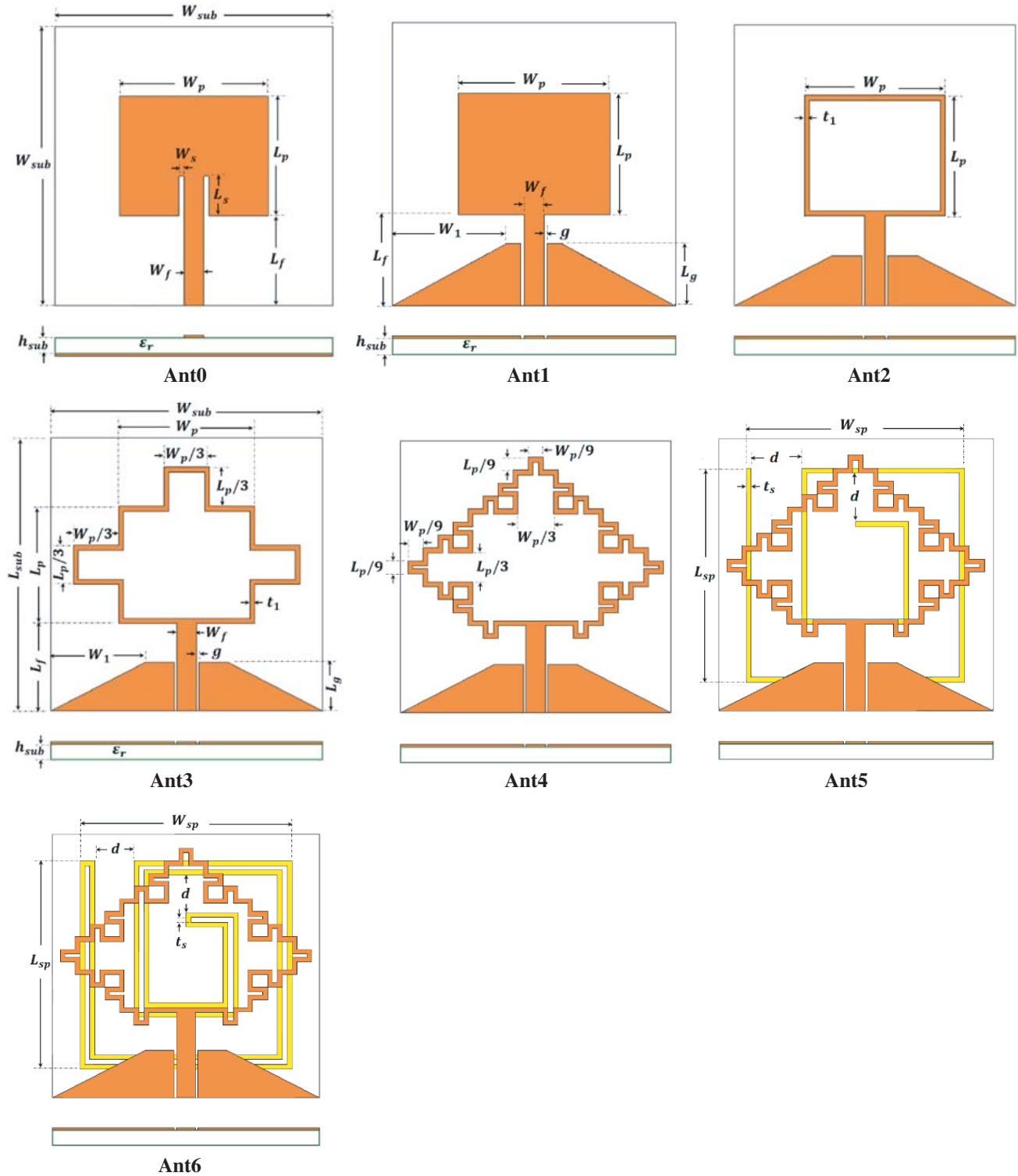
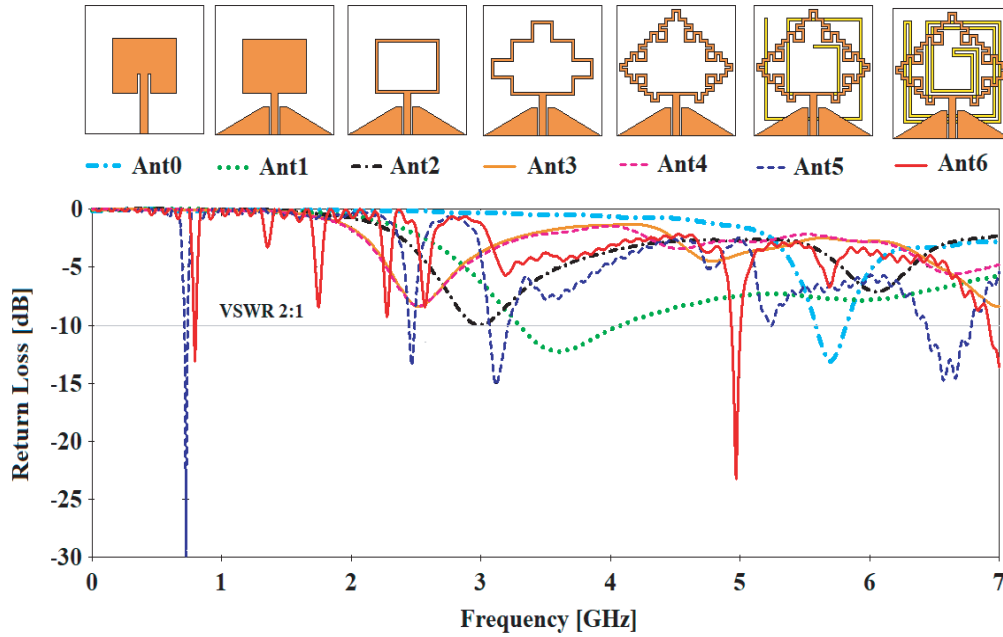


Figure 4. The evolution design procedure for the proposed antenna.

### 3.3. Design of the Conventional MPA

Conventional strip-fed rectangular MPA is the best structure to begin with for designing the proposed initial antenna to operate at different frequency bands. In this section, the transmission line model,



**Figure 5.** Simulated return loss characteristics for antennas.

Eqs. (13)–(16) [38], is used to design MPA to operate at the desired resonance frequency  $f_r = 5.8$  GHz (RFID/WLAN band) by assuming the relative permittivity  $\epsilon_r = 4.3$  (FR4) and the height of the substrate  $h_{sub} = 1.6$  mm.

$$\epsilon_{eff} = \frac{\epsilon_r + 1}{2} + \frac{\epsilon_r - 1}{2} \left( \frac{1}{\sqrt{1 + 12h/W_p}} \right) \quad (13)$$

where  $(\epsilon_r, h, W_p)$  are the dielectric constant, height of the substrate, and width of the patch, respectively. The patch length and width of the antenna identify antenna resonance. The patch length ( $L_p$ ) of the antenna for dominant mode resonance is given as:

$$L_p = \frac{1}{2f_r \sqrt{\epsilon_{eff}} \sqrt{\mu_0 \epsilon_0}} - 2\Delta L_p \quad (14)$$

where,

$$\Delta L_p = 0.412h \frac{(\epsilon_{eff} + 0.300) \left( \frac{W_p}{h} + 0.262 \right)}{(\epsilon_{eff} - 0.258) \left( \frac{W_p}{h} + 0.813 \right)} \quad (15)$$

The width of the patch antenna is given by

$$W_p = \frac{c}{2f_r} \sqrt{\frac{2}{\epsilon_r + 1}} \quad (16)$$

Here  $c$  is the speed of light in space, and  $f_r$  is the resonance frequency of the antenna. As a result, the calculated patch length and width are, respectively, ( $L_p = 11.06$  mm) and ( $W_p = 15.88$  mm). Then, a pair of slots with length  $L_s$  and width  $W_s$  is cut from the conventional MPA, and this yields Ant0 as illustrated in Figure 6(a). Later on, Ant0 is simulated by using CST MWS with  $L_p = 11.06$  mm and  $W_p = 15.88$  mm as initial values to begin with. After that, by fine-tuning the antennas' geometrical parameters, Ant0 operates at  $f_r = 5.7$  GHz with a magnitude of return loss less than  $-13$  dB, and the maximum gain radiation pattern is nearly 4 dB at the front direction of the antenna as noticed in Figure 6(b). This antenna has patch dimensions  $L_p \times W_p$  of 12 mm  $\times$  15 mm, and its total substrate dimensions are (28 mm  $\times$  28 mm).

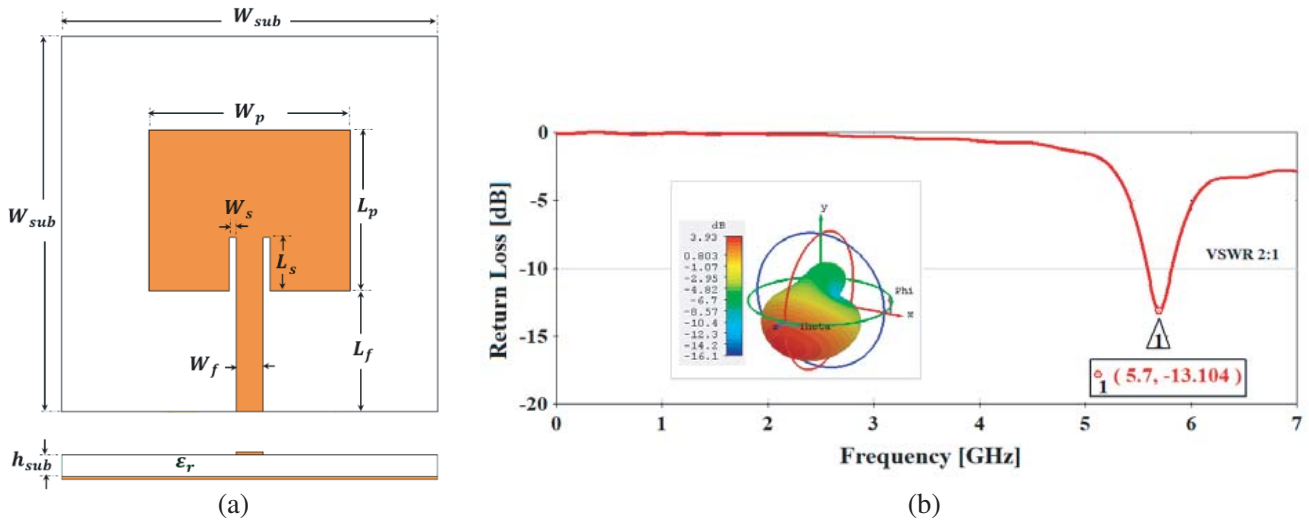


**Figure 6.** (a) Conventional microstrip inset-fed MPA, Ant0 and (b) its return loss and radiation pattern.

**3.4. Design of the Tapered CPW-fed MPA**

After that conventional MPA (Ant0) was designed to operate at  $f_r = 5.8$  GHz, Ant0 is redesigned after replacing its inset fed by the counterpart CPW-fed with the tapered ground plane, and consequently Ant1 is produced as shown in Figure 7(a). As noticed from the  $S_{11}$  plot, Figure 7(b), Ant1 resonates at  $f_{r1} \cong 3.6$  GHz with return loss of approximately  $-12$  dB, in addition to  $f_{r2} \cong 5.9$  GHz presented in the conventional MPA but with return loss greater than  $-10$  dB. The overall dimension  $L_{sub} \times W_{sub}$  of the antenna is  $28 \text{ mm} \times 28 \text{ mm}$  whereas its patch size  $L_p \times W_p$  is  $12 \text{ mm} \times 14 \text{ mm}$ .

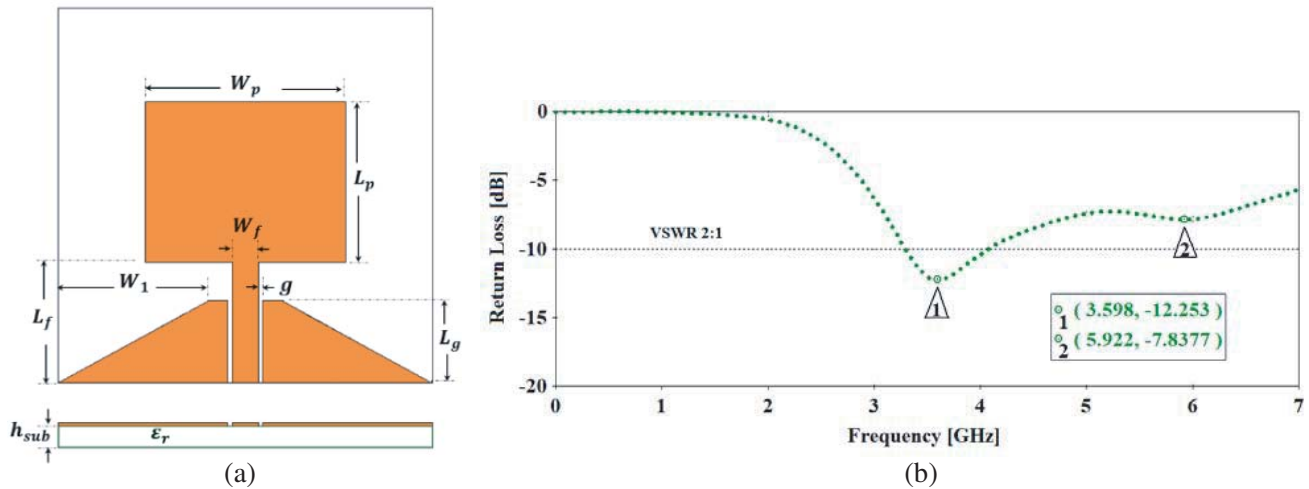


**Figure 7.** (a) Tapered CPW-fed MPA, (Ant1) and (b) its return loss characteristic.

**3.5. Design of the Minkowski Fractal Antenna**

This section describes the evolution process for designing Ant2, Ant3, and Ant4, which are called, respectively, zero-, first-, and second-order Minkowski fractal antennas, MFA0, MFA1, and MFA2. These three antennas are shown in Figure 8.

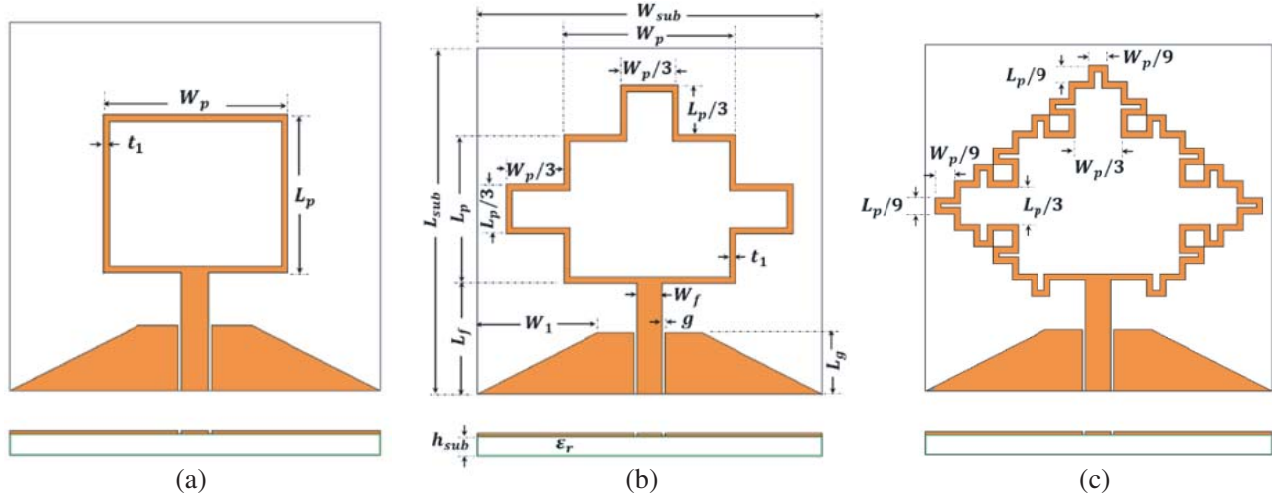


**Figure 8.** Tapered CPW-fed Minkowski fractal antenna (MFA). (a) MFA0. (b) MFA1. (c) MFA3.

The MFA0, as seen in Figure 8(a) is evolved from Ant1 by replacing its patch structure with the counterpart patch strip of thickness  $t_1 = 0.5$  mm. Then, MFA1 is obtained by adding three medium size rectangular strips of length  $(L_p/3) \times (W_p/3)$  to the right, left, and upper sides of the large rectangular strip of MFA0, see Figure 8(b). After that, MFA2 as depicted in Figure 8(c) can be produced by adding three of small strips with length  $(L_p/9) \times (W_p/9)$  to the three medium strips of MFA1, and other eight of such small strips are added to its main rectangular strip with two strips for each one of the four sides. The return loss curves of these antennas are plotted in Figure 9. It is seen from this figure that Ant2 (Ant3) resonates at two frequencies 3 GHz and 6 GHz (2.5 GHz and 4.8 GHz) whereas Ant3 resonates at three frequencies, 2.5, 4.5 and 6.6 GHz.

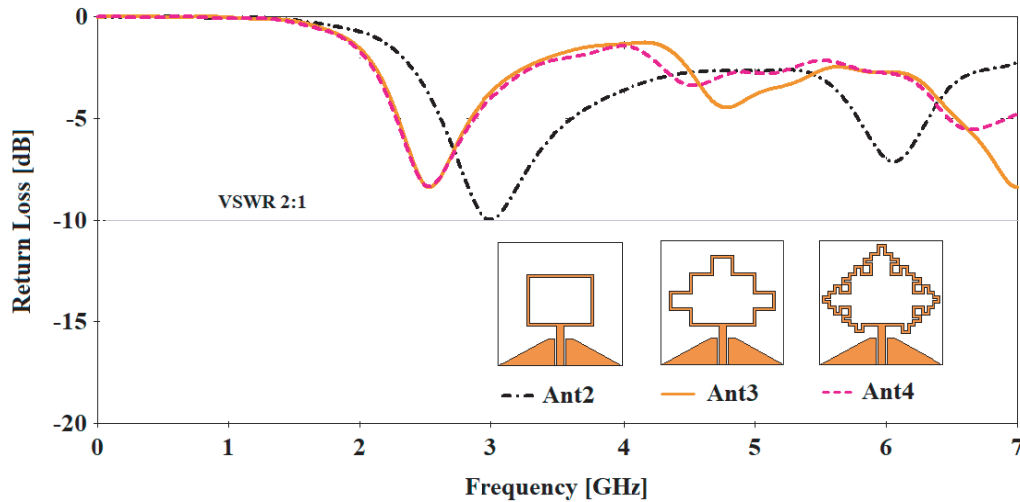


**Figure 9.** Simulated return loss characteristics for Tapered CPW-fed Minkowski fractal antenna (MFA). (a) MFA0 or Ant2. (b) MFA1 or Ant3. (c) MFA2 or Ant4.

All resonance frequencies of these three antennas have return loss values above  $-10$  dB. Hence, it is required to add another structure to the MFA2 (Ant4) in order to have the desired five frequency bands suitable for using in modern wireless communications. This is done by adding a spiral loop strip structure in the back substrate of Ant4. The next section describes this process for achieving initialized antenna that satisfies the aforementioned requirement.

### 3.6. Design of the Minkowski Fractal- and Spiral-Based Antenna

As discussed in the previous subsection, it is required to add other structure to the designed antenna, MFA2 to operate at multiple frequencies covering the desired bands. The spiral structure is a appropriate solution to do that duo to its ability to add more resonance frequencies to the original designed antenna by sufficiently selecting their geometrical parameters, spiral width and length,  $L_{sp}$  and  $W_{sp}$ , besides its thickness  $t_2$ , spacing between strips  $W_2$ , and loop length  $L_1$ . Figure 10 shows the proposed initial designed antenna after adding the spiral geometry (colored as yellow) in the back side of the FR4 substrate.

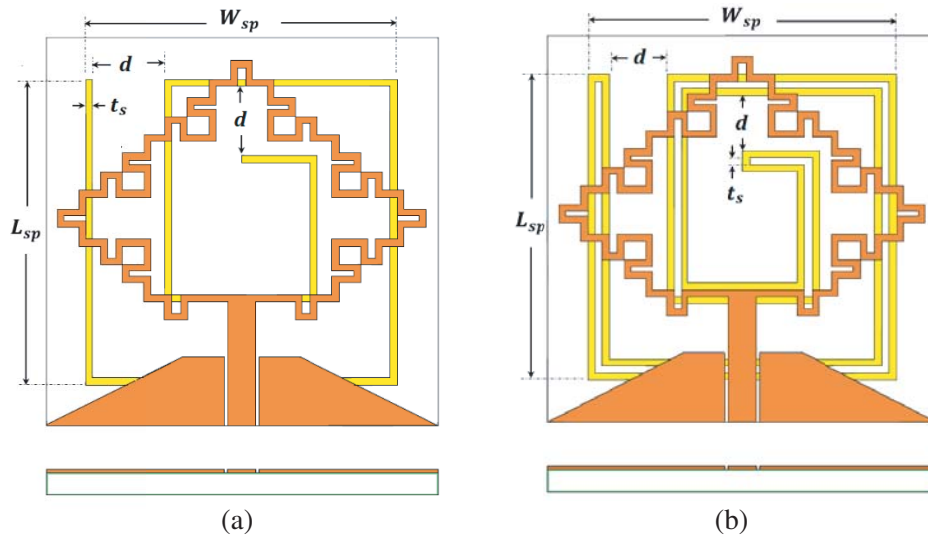


**Figure 10.** Tapered CPW-fed Minkowski fractal- and spiral-based antenna (MFSA). (a) MFSA1. (b) MFSA2.

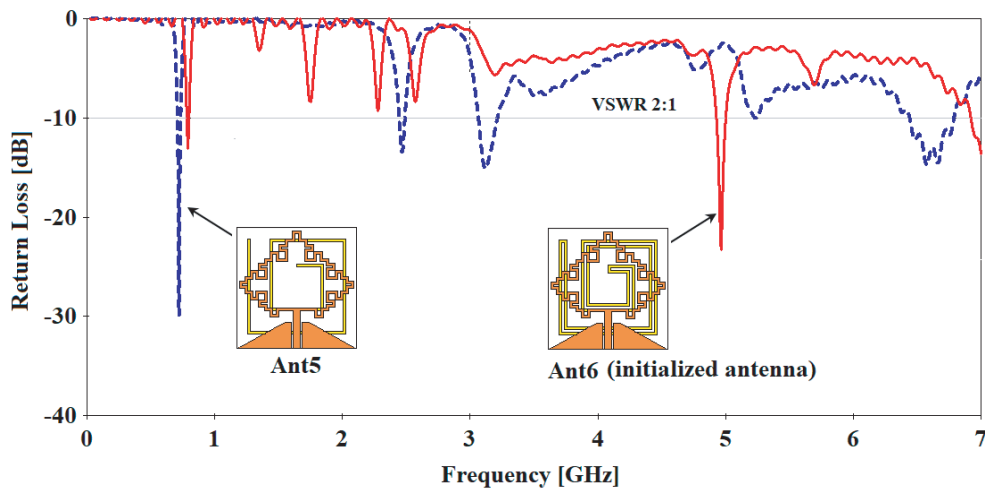


**Figure 11.** Simulated return loss characteristics for Tapered CPW-fed Minkowski fractal- and spiral-based antenna (MFSA).

The simulated return losses for Ant5 and Ant6 are plotted in Figure 11. As seen from this figure, Ant5 resonates at six frequencies, 0.72, 2.46, 3.11, 4.76, 5.24, and 6.57 GHz whereas Ant6 resonates at eight frequencies, including 0.79, 1.35, 1.75, 2.27, 2.57, 3.20, 4.97, and 5.7 GHz. As a result, although Ant6 represents the final structure of the evolution process starting from the conventional MPA, it is

capable of operating at different frequencies, but these frequencies do not meet the desired frequencies. Thus, it is required to fine-tune these bands obtained from the initial designed antenna (Ant6) by using the optimization design methodology described earlier. The following section discusses in details the application of the design methodology for the initialized designed antenna (MFSA) to yield an optimized antenna having appropriate frequency bands.

#### 4. DESIGN OF THE OPTIMIZED ANTENNA

This section presents the application of the objective function described in the previous section to the initial designed antenna for covering the desired  $K$ -frequency bands. For each  $j$ th band ( $1 \leq j \leq K$ ), the  $j$ th lower and higher frequencies  $f_{Lj}$  and  $f_{Hj}$ , respectively, are required to be within the maximum and minimum of lower and higher frequencies  $f_{dLj}$  and  $f_{dHj}$ , i.e.,  $f_{dLj}^{\min} \leq f_{Lj} \leq f_{dLj}^{\max}$  and  $f_{dHj}^{\min} \leq f_{Hj} \leq f_{dHj}^{\max}$ . Tables 2 and 3 illustrate the frequency band used in wireless communications and the counterpart desired bands defined in the optimization methodology, respectively, for five desired bands,  $K = 5$ .

**Table 2.** Frequency bands (in MHz) considered for wireless communications.

Band number $j$	Application	Lower frequency $f_{Lj}$	Center frequency $f_{Cj}$	Higher frequency $f_{Hj}$
1	UHF RFID	860	910	960
2	GSM	1700	1760	1820
3	ISM, RFID	2400	2450	2500
4	WiMAX	3300	3450	3600
5	ISM, RFID	5725	5800	5875

**Table 3.** The desired Frequency bands (in MHz) used in optimization methodology.

Band number $j$	Lower desired frequency			Higher desired frequency		
	$f_{dLj}$	$f_{dLj}^{\min}$	$f_{dLj}^{\max}$	$f_{dHj}$	$f_{dHj}^{\min}$	$f_{dHj}^{\max}$
1	860	840	860	920	920	940
2	1760	1700	1760	1800	1800	1820
3	2390	2390	2420	2450	2450	2460
4	3300	3000	3300	3600	3600	3800
5	5725	5680	5725	5875	5875	5900

The initialized antenna designed in the previous sections is replotted here, as shown in Figure 12, to optimize it by utilizing the design procure discussed in Section 3, for satisfying the desired frequency bands described in Table 2. As seen from Figures 12(a) and (b), the two structures, fractal and spiral, are printed on the front and back sides of the FR4 substrate, respectively, with dimensions (Length  $\times$  Width  $\times$  Height) of  $(L_{\text{sub}} \times W_{\text{sub}} \times h_{\text{sub}})$ . Table 4 illustrates the geometrical parameters of the optimized designed antenna which do not change during the optimization whereas Table 5 lists the geometrical parameters allowed to be varied within the specified range of values.

To prevent occurring of any physically invalid antenna structures during the optimization process, the fractal patch geometrical parameters ( $L_p$  and  $W_p$ ) are allowed to be changed as scaling factors ( $K_{Lp}$  and  $K_{Wp}$ ), respectively, related to the main fixed parameters, substrate length  $L_{\text{sub}}$  or substrate width  $W_{\text{sub}}$  (since  $L_{\text{sub}} = W_{\text{sub}} = 28$  mm, square MPA). These scale factors are given by:

$$K_{Lp} = L_p / L_{\text{sub}} \quad \text{or} \quad L_p = 28 \times K_{Lp} \tag{17a}$$

$$K_{Wp} = W_p / L_{\text{sub}} \quad \text{or} \quad W_p = 28 \times K_{Wp} \tag{17b}$$

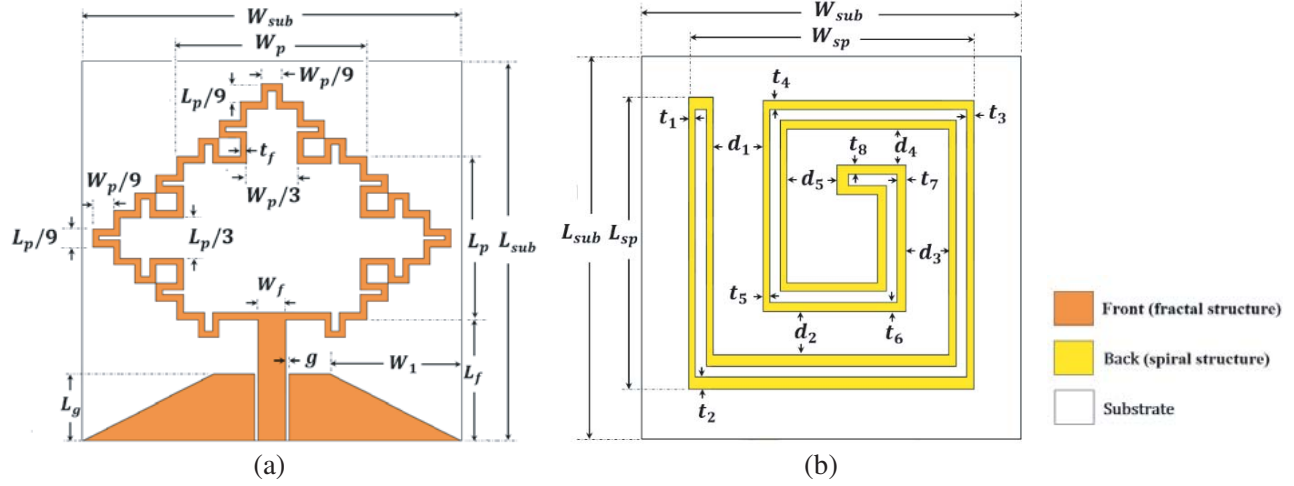


Figure 12. Geometry of the proposed optimized designed antenna. (a) Front side. (b) Back side.

Table 4. Antenna geometrical parameters that remain unchanged during optimization.

No.	Parameter	Symbol	Value (mm)
1	Substrate length	$L_{sub}$	28.0
2	Substrate width	$W_{sub}$	28.0
3	Substrate height	$h_{sub}$	1.5
4	Feeding width	$W_f$	2.0
5	CPW gap width	$g$	0.25
6	Fractal strip thick	$t_f$	0.5
7	Spiral length	$L_{sp}$	21.0
8	Spiral width	$W_{sp}$	21.0
9	Spiral distance	$d_{sp}$	0.8

Table 5. Ranges of the design parameters used for the optimizing MFSA.

No.	Parameter	Ranges (mm)	No.	Parameter	Ranges (mm)
1	$t_1$	0.3 ~ 0.6	8	$t_8$	0.4 ~ 0.8
2	$t_2$	0.6 ~ 0.9	9	$d_1$	2.9 ~ 4.6
3	$t_3$	0.3 ~ 0.6	10	$d_2$	2.6 ~ 4.3
4	$t_4$	0.4 ~ 0.8	11	$d_3$	2.9 ~ 4.6
5	$t_5$	0.4 ~ 0.6	12	$d_4$	2.75 ~ 4.4
6	$t_6$	0.4 ~ 0.8	13	$d_5$	2.8 ~ 4.6
7	$t_7$	0.4 ~ 0.8			

The reason behind the changing of these two parameters only and not allowing the spiral parameters  $L_{sp}$  and  $W_{sp}$  to be varied during the optimization process is that these parameters do not markedly affect the antenna performance as noticed in designing the initialized antenna. The ranges of these two scale parameters are listed in Table 6.

As seen from Tables 5 and 6, fifteen geometrical parameters, i.e.,  $N_g = 15$  dimensions, enter the optimization process, two as scaling parameters and the remaining thirteen as geometrical parameters. In order to obtain a good convergence with relatively less processing time, it is appropriate to select both

**Table 6.** Ranges of the scaling parameters for the optimized antenna.

No.	Scale parameter	Range	Dimension parameter	Range (mm)
1	$K_{W_p}$	0.35 ~ 0.53	$L_p = 28 \times K_{L_p}$	9.80 ~ 14.84
2	$K_{L_p}$	0.4 ~ 0.6	$W_p = 28 \times K_{W_p}$	11.20 ~ 16.80

the maximum number of iterations and PSO particles for each iteration depending on the dimension of the solution space  $N_g$ . Thus, to compromise between the good convergence and acceptable processing time, the best choice of PSO particles ( $N_p$ ) used in this work is between  $3N_g$  and  $5N_g$ . Thus, for  $N_g = 15$ ,  $N_p = 45$ -particle swarms for PSO algorithm and total of 100 iterations are used for optimizing the proposed antenna. Furthermore, a stopping criterion is chosen such that either the objective function is satisfied  $F(\mathbf{x}) = -5$  (five desired bands) or 100 PSO iterations are reached, i.e., 4500- $S_{11}$  results are offered by CST simulator program.

### 5. RESULTS RELATED TO THE OPTIMIZED ANTENNA

This section investigates and discusses in details the simulated and measured impedance bandwidth results related to the optimized antenna. The simulated surface current distributions at resonant modes in addition to the optimized geometrical parameters of the proposed antenna are also presented.

#### 5.1. Optimized Geometrical Parameters and Antenna Performance

The PSO algorithm produces an optimized antenna having the final geometrical parameters listed in Table 7. The simulated return loss characteristics of the initial and optimized antennas are shown in Figure 13. As noticed from this figure, the optimized antenna nearly operates at the desired bands. The

**Table 7.** The geometrical parameters of optimized antenna (Units: in mm).

<b>Parameter</b>	$t_1$	$t_2$	$t_3$	$t_4$	$t_5$
<b>Value</b>	0.5	0.85	0.5	0.65	0.45
<b>Parameter</b>	$t_6$	$t_7$	$t_8$	$d_1$	$d_2$
<b>Value</b>	0.65	0.65	0.65	3.70	3.35
<b>Parameter</b>	$d_3$	$d_4$	$d_5$	$L_p$	$W_p$
<b>Value</b>	3.20	3.05	3.75	12.60	13.70

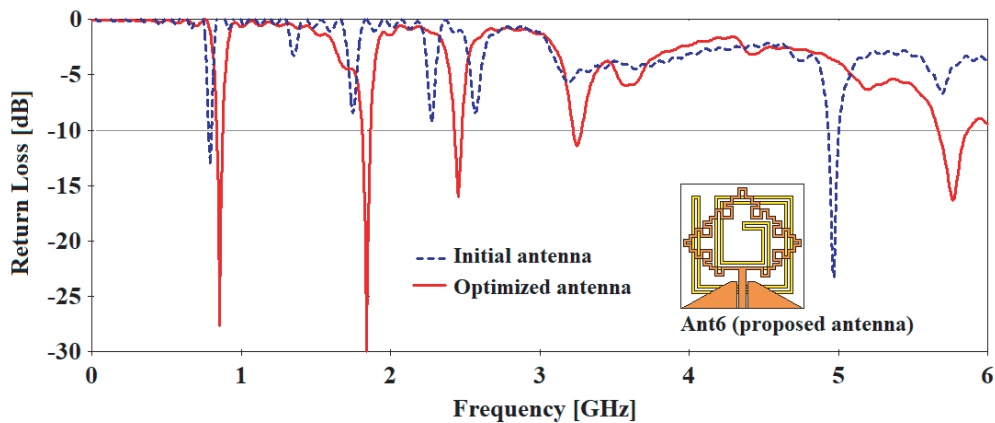


**Figure 13.** Simulated return loss characteristics of the initial and optimized antennas.

next section investigates in details a discussion for the simulated and measured results of the proposed optimized antenna.

## 5.2. Experimental Results and Discussion

Having successfully completed the optimization methodology for designing antennas to cover the desired frequency bands, the antenna prototype with optimized dimensions in Table 7 has been fabricated. The proposed antenna is tested using Agilent/HP N9923A 6 GHz Handheld RF Vector Network Analyzer. The simulated and measured return loss characteristics of the initial and optimized antenna are shown in Figure 14. This figure clarifies the effectiveness of the proposed design methodology for fine-tuning the  $-10$  dB impedance bandwidths of the optimized antenna to cover the desired frequency bands. Table 8 summarizes the simulated and measured five frequency bands in terms of  $j$ th lower, higher, and resonance frequency  $f_{Lj}$ ,  $f_{Hj}$ , and  $f_{rj}$ , respectively.

**Table 8.** The simulated and measured frequency bands of optimized antenna (in MHz).

Band number $j$	Simulation result			Measurement result		
	$f_{Lj}$	$f_{Hj}$	$f_{rj}$	$f_{Lj}$	$f_{Hj}$	$f_{rj}$
1	840	876	856	768	998	864
2	1810	1867	1840	1810	1868	1848
3	2430	2480	2450	2242	2475	2.34
4	3223	3280	3250	3327	3438	3380
5	5665	5870	5770	5725	5920	5830

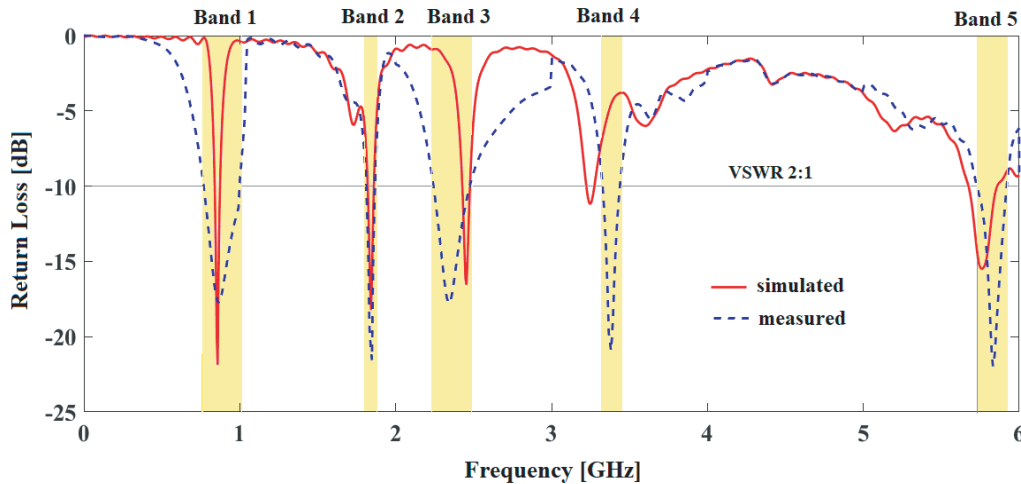


**Figure 14.** Simulated return loss characteristics of the initial and optimized antennas.

It is demonstrated from Table 8 and Figure 14 that the measured  $-10$ -dB  $j$ th bandwidth,  $BW_j = f_{Hj} - f_{Lj}$  ( $f_{Lj}$  to  $f_{Hj}$ ) of the optimized antenna are 230 MHz (768 to 998 MHz), 58 MHz (1810 to 1868 MHz), 233 MHz (2242 to 2475 MHz), 111 MHz (3327 to 3438 MHz), and 195 MHz (5725 to 5920 MHz). It is clear from this figure that the measured and simulated results show a good agreement for the three lower bands (Band 1, Band 2, and Band 3), but they nearly coincide with each other at the two higher bands (Band 4 and Band 5). Also, these simulated and measured return loss curves reveal that there is a slight deviation in the resonance frequencies which may be attributed to some factors such as manufacturing imperfection, SMA soldering, substrate misalignment, thickness, and/or dielectric constant.

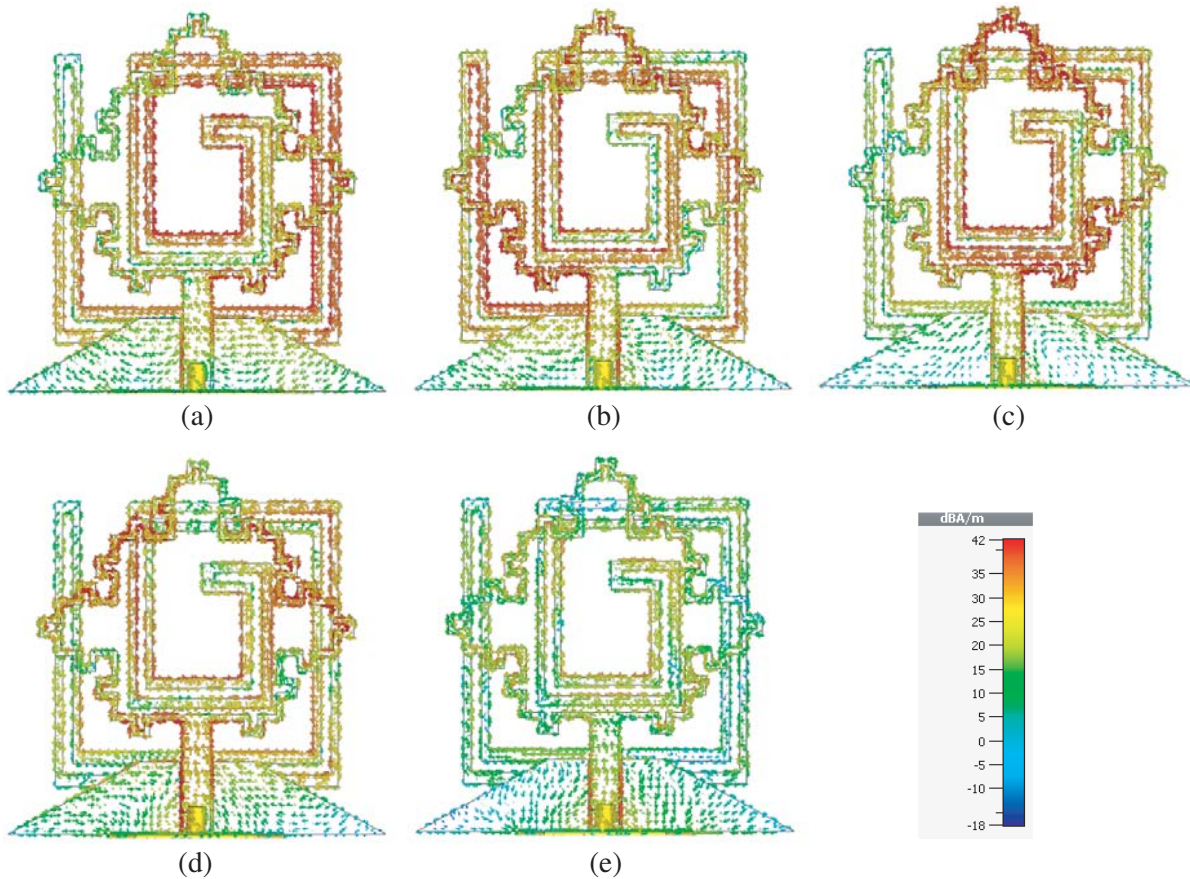


**Figure 15.** Distribution of surface currents at (a) 850 MHz, (b) 1840 MHz, (c) 2450 MHz, (d) 3250 MHz and (e) 5770 MHz.

To clarify the multiband characteristic of the optimized antenna, the surface current distributions at resonant modes are depicted in Figure 15. This figure demonstrates the simulated surface current distributions at five resonant frequencies of 850, 1840, 2450, 3250, and 5770 MHz, respectively. It is seen from Figures 15(a) and (b) that at the frequencies of 850 and 1840 MHz, the current is concentrated along the outer/inner edges of spiral strip, and the density of current gets lower value at the fractal strip. On the other hand, the surface currents at 2450 and 3250 MHz, in Figures 15(c) and (d), are mainly concentrated at the inner edges of spiral and fractal strips. Finally, at the higher frequency of 5770 MHz, the surface current flows along the edge of CPW strip and perimeter of ground plane. This clearly demonstrates that the spiral strip structure is responsible for enhancing the impedance matching of the proposed antenna at lower resonant modes as stated in the previous section.

## 6. FAR-FIELD ANTENNA PERFORMANCE AND COMPARISON WITH OTHER PUBLISHED ANTENNAS

The far-field performance in terms of realized peak gain and efficiency of the proposed antenna is presented in this section. The comparison of this antenna with published antennas in terms of size and frequency bands is also presented.

### 6.1. Realized Peak Gain and Efficiency

The realized peak gain and efficiency versus frequency for the optimized antenna at five resonance frequency modes of 850, 1840, 2450, 3250, and 5770 MHz are shown in Figures 16(a) and (b), respectively.

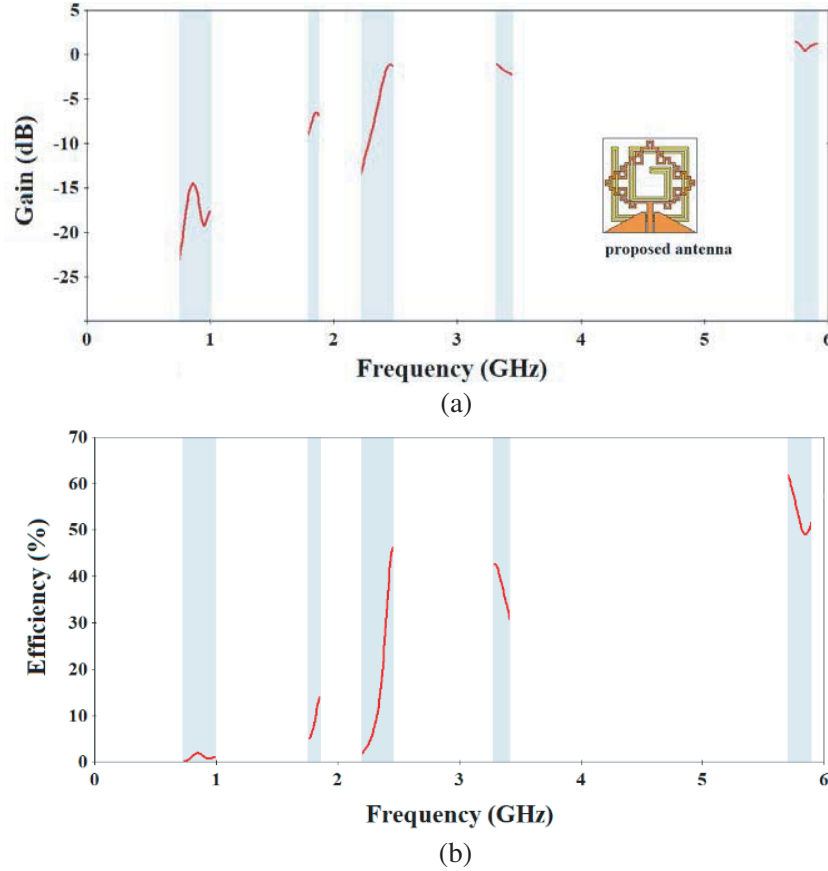


**Figure 16.** The (a) peak gain and (b) efficiency of the proposed antenna.

**Table 9.** The simulated realized peak gain and efficiency of optimized antenna at five resonance frequencies.

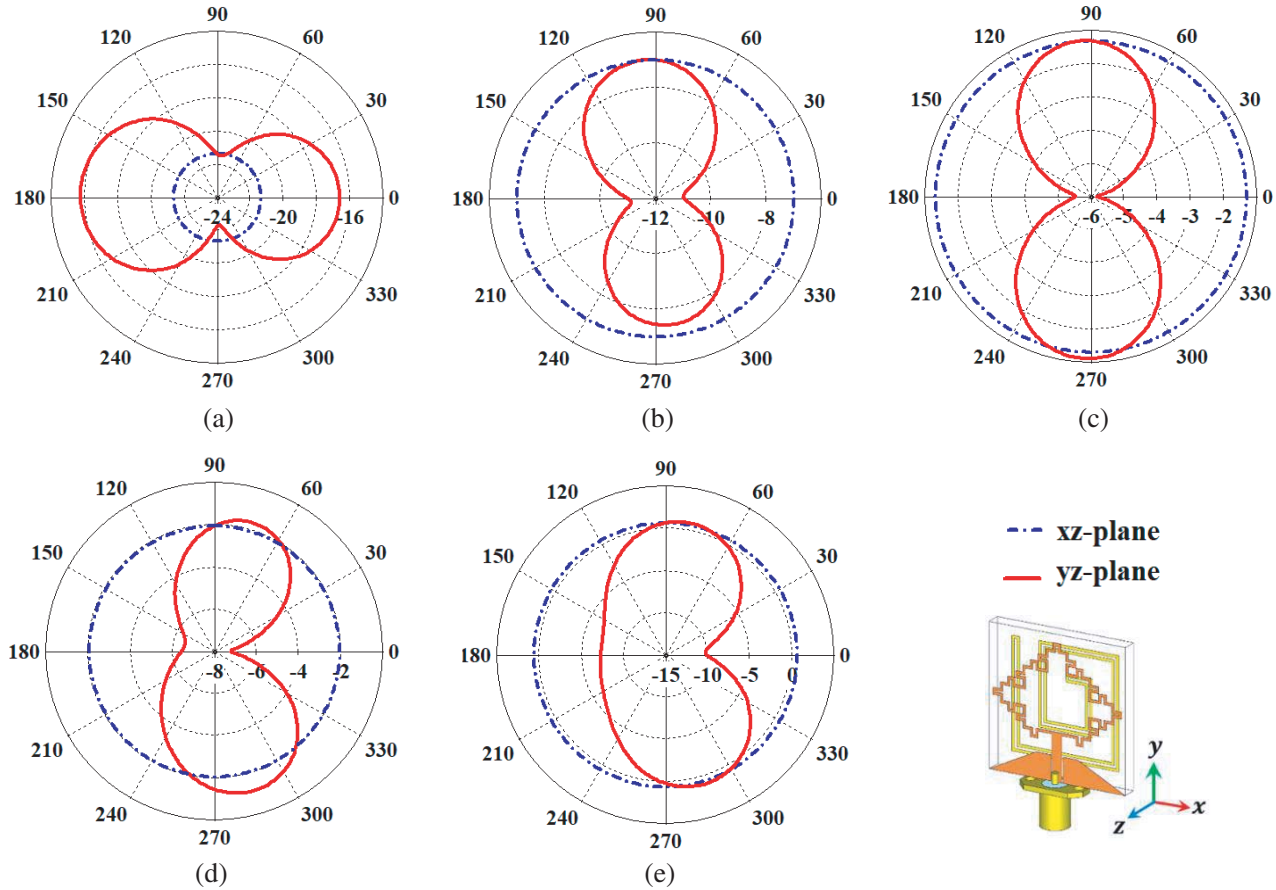
Band number $j$	1	2	3	4	5
Resonance Frequency (MHz)	850	1840	2450	3250	5770
Gain (dB)	-14.45	-6.60	-1.00	-0.83	1.58
Efficiency (%)	1.93	13.90	46.62	42.22	62.88

Table 9 lists the peak gain and efficiency for the proposed antenna at the aforementioned resonance frequencies.

It is seen from Figure 16 and Table 9 that the antenna peak gain and efficiency are increased with increase of operating frequency. The gain (efficiency) is  $-14.45$  dB (1.93%) at the 1st resonant frequency  $f_{r1} = 850$  MHz and increases to become 1.58 dB (62.88%) at the 5th resonant frequency  $f_{r5} = 5770$  MHz. The reason behind the above results in significantly reduction in antenna gain and efficiency throughout the lower frequency bands is that the antenna radiation depends on operating frequency. On the other hand, the proposed antenna has miniaturized physical size which makes wavelengths of lower frequencies become smaller than antenna dimensions, and hence EM energy is unable for radiation to the free space.

## 6.2. Radiation Pattern

This section presents the simulated 2D and 3D radiation patterns for the proposed antenna. Figure 17 shows the simulated 2D radiation patterns of the proposed antenna including the principle planes:  $E$ -



**Figure 17.** 2D radiation patterns of optimized antenna at (a) 850 MHz, (b) 1840 MHz, (c) 2450 MHz, (d) 3250 MHz and (e) 5770 MHz.

plane ( $y$ - $z$  plane) and  $H$ -plane ( $x$ - $z$  plane). These two planes are plotted for five resonance frequencies 850, 1840, 2450, 3250, and 5770 MHz. It is clear from this figure that the radiation patterns in  $H$ -plane have almost symmetrically stable omnidirectional patterns throughout the five operating frequencies. On the other hand, the  $E$ -plane radiation patterns are nearly symmetrical and omnidirectional.

The 3D radiation patterns for the aforementioned operating frequencies are presented in Figure 18. It is concluded from this figure that the proposed antenna has nearly stable and omnidirectional radiation patterns for the five frequencies.

### 6.3. Comparison with Antennas Reported in the Literature

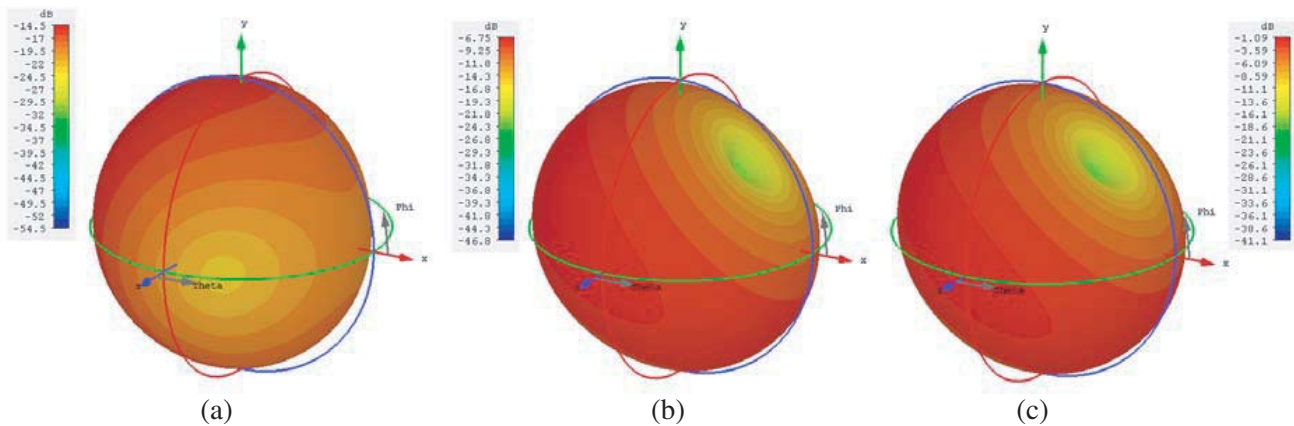
Table 10 lists a performance comparison between the optimized antenna presented in this work and some multiband antennas published in recent references. It is clear from this comparison that the proposed antenna has a total area  $A_{\text{Work}}$  of just  $748 \text{ mm}^2$  or  $0.0053\lambda_0^2$ , where  $\lambda_0$  is the free space wavelength at the first lower frequency, which is a smaller area than all published areas  $A_{\text{Pub}}$  of the antennas listed in this table. The criterion used for area reduction  $r_{\text{Area}}$  is computed as

$$r_{\text{Area}}(\%) = \left[ 1 - \frac{A_{\text{Work}} \text{ (in } \lambda_0^2 \text{)}}{A_{\text{Pub}} \text{ (in } \lambda_0^2 \text{)}} \right] \times 100\% \tag{18}$$

It can be seen that by applying Eq. (18) for antennas published in Table 10 resulting area reduction ranges from 28.38% to 95.26% for antennas reported in [13] and [5], respectively. Thus, the proposed antenna is characterized by covering multiband frequency bands with a smaller area or percentage of area reduction than the antennas presented in the previous literature.

**Table 10.** A comparison between recent published multiband antennas and the proposed antenna in this chapter.

[Ref]	Physical size, $L_{sub} \times W_{sub}$ (mm <sup>2</sup> )	Electrical size, $L_{sub} \times W_{sub}$ , [ $\lambda_0^2$ ]	Operating bands, or centre frequency [MHz]	Total area reduction [%]
[5]	105 × 175 18375 mm <sup>2</sup>	0.4317 × 0.2590, 0.1118 $\lambda_0^2$	740 2450 3500 5800	95.26%
[12]	30 × 30 900 mm <sup>2</sup>	0.0945 × 0.0945, 0.0089 $\lambda_0^2$	945 2500 3520 5800	40.45%
[13]	40 × 32 1280 mm <sup>2</sup>	0.0768 × 0.096, 0.0074 $\lambda_0^2$	720 3100 5580	28.38%
[15]	72 × 72 5184 mm <sup>2</sup>	0.216 × 0.216, 0.0467 $\lambda_0^2$	810–1070 1590–2450	88.65%
[16]	17 × 16 272 mm <sup>2</sup>	0.136 × 0.128, 0.0174 $\lambda_0^2$	2400 3600 5500	69.54%
[20]	72 × 72 5184 mm <sup>2</sup>	0.216 × 0.216, 0.0467 $\lambda_0^2$	900 1600 1800 2450	88.65%
[22]	77 × 26 2002 mm <sup>2</sup>	0.231 × 0.078, 0.018 $\lambda_0^2$	900 2400 5800	70.55%
<b>This work</b>	28 × 28 784 mm <sup>2</sup>	0.078 × 0.078, 0.0053 $\lambda_0^2$	768–998 1810–1868 2242–2475 3327–3438 5725–5920	



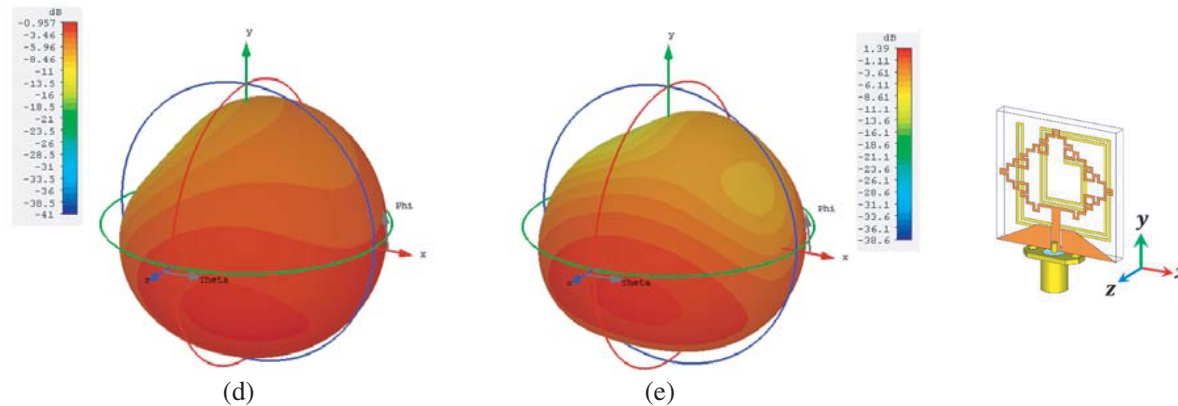


**Figure 18.** 3D radiation patterns of optimized antenna at (a) 850 MHz, (b) 1840 MHz, (c) 2450 MHz, (d) 3250 MHz and (e) 5770 MHz.

## 7. CONCLUSION

A new two-step optimization methodology that focuses on designing multiband antenna under miniaturized size has been proposed. Twofold benefits of this work compared with the widely used optimization methods have been obtained. This work is presented for the first time, and a general objective function successfully makes an optimized antenna for covering the all desired frequency bands. This is done by introducing the objective function terms related to the specified  $-10$  dB  $S_{11}$  lower and higher frequencies. The optimization approaches used in the previous studies for multiband antenna design are restricted and are not as accurate as they should be. To demonstrate competence of the optimization approach, a dual-antenna structure, having an overall dimensions of just  $28 \text{ mm} \times 28 \text{ mm}$ , has been optimized for operating in different five-bands covering most sub-6 GHz international standard. Simulated and measured results demonstrate that the proposed antenna successfully satisfies the desired five frequency bands. Based on the experimental results, these bands are: (768–998 MHz), (1810–1868 MHz), (2242–2475 MHz), (3327–3438 MHz), and (5725–5920 MHz) which are compatible with the RFID, GSM, WLAN, and WiMAX applications. Furthermore, omnidirectional radiation patterns with somewhat satisfactory gains and efficiencies make it an appropriate candidate as an internal antenna for multiband wireless communication systems.

## ACKNOWLEDGMENT

The authors would like to thank Dr. Ghassan N. Jawad from the University of Baghdad for providing the measurement results and Prof. Raad S. Fyath from Al-Nahrain University for his assistance for improving this manuscript.

## REFERENCES

1. Bashir, U., K. R. Jha, G. Mishra, G. Singh, and S. K. Sharma, "Octahedron-shaped linearly polarized antenna for multistandard services including RFID and IoT," *IEEE Trans. Antennas Propag.*, Vol. 65, No. 7, 3364–3373, 2017.
2. Attaran, A. and R. Rashidzadeh, "Chipless radio frequency identification tag for IoT applications," *IEEE Internet of Things Journal*, Vol. 3, No. 6, 1310–1318, 2016.
3. Lizzi, L., F. Ferrero, P. Monin, C. Danchesì, and S. Boudaud, "Design of miniature antennas for IoT applications," *2016 IEEE Sixth International Conference on Communications and Electronics (ICCE)*, 234–237, 2016.
4. Saha, T. K., T. N. Knaus, A. Khosla, and P. K. Sekhar, "A CPW-fed flexible UWB antenna for IoT applications," *Microsyst. Technol.*, 1–7, December 2018.

5. Lukasz, J., D. B. Paolo, J. Lukasz, and H. Slawomir, "Many-objective automated optimization of a four-band antenna for multiband wireless sensor networks," *Sensors*, Vol. 18, 3309, 2018.
6. Januszkiewicz, L., P. Di Barba, and S. Hausman, "Optimization of wearable microwave antenna with simplified electromagnetic model of the human body," *Open Phys.*, Vol. 15, 1055–1060, 2017.
7. Yang, H., W. Yao, Y. Yi, X. Huang, S. Wu, and B. Xiao, "A dual-band low-profile metasurface-enabled wearable antenna for WLAN devices," *Progress In Electromagnetics Research C*, Vol. 61, 115–125, 2016.
8. Wang, B. and W. Wang, "A miniature tri-band RFID reader antenna with high gain for portable devices," *International Journal of Microwave and Wireless Technologies*, Vol. 9, No. 5, 1163–1167, June 2017.
9. Zhang, T., R. Li, G. Jin, G. Wei, and M. Tentzeris, "A novel multiband planar antenna for GSM/UMTS/LTE/Zigbee/Rfid mobile devices," *IEEE Trans. Antennas Propag.*, Vol. 59, No. 11, 4209–4214, November 2011.
10. Li, H., Y. Zhou, X. Mou, Z. Ji, H. Yu, and L. Wang, "Miniature four-band CPW-fed antenna for RFID/WiMAX/WLAN applications," *IEEE Antennas Wireless Propag. Lett.*, Vol. 13, 1684–1688, 2014.
11. Guan, Y., Z. Zhou, Y. Li, and H. Xiao, "A novel design of compact dipole antenna for 900 MHz and 2.4 GHz RFID tag applications," *Progress In Electromagnetics Research Letters*, Vol. 45, 99–104, 2014.
12. Panda, J. R. and R. S. Kshetrimayum, "A printed 2.4 GHz/5.8 GHz dual-band monopole antenna with a protruding stub in the ground plane for WLAN and RFID applications," *Progress In Electromagnetics Research*, Vol. 117, 425–434, 2011.
13. Ghosh, S. K. and R. K. Badhai, "Spiral shaped multi frequency printed antenna for mobile wireless and biomedical applications," *Wireless Personal Communications*, Vol. 98, No. 3, 2461–2471, February 2018.
14. Salim, M. and A. Pourziad, "A novel reconfigurable spiral-shaped monopole antenna for biomedical applications," *Progress In Electromagnetics Research Letters*, Vol. 57, 79–84, 2015.
15. Kerkhoff, A. J., R. L. Rogers, and H. Ling, "Design and analysis of planar monopole antennas using a genetic algorithm approach," *IEEE Trans. Antennas Propag.*, Vol. 52, No. 10, 2709–2718, 2004.
16. Griffiths, L. A., C. Furse, and Y. C. Chung, "Broadband and multiband antenna design using the genetic algorithm to create amorphous shapes using ellipses," *IEEE Trans. Antennas Propag.*, Vol. 54, No. 10, 2776–2782, October 2006.
17. Fertas, K., H. Kimouche, M. Challal, H. Aksas, and R. Aksas, "An optimized shaped antenna for multiband applications using Genetic Algorithm," *4th International Conference on Electrical Engineering (ICEE)*, 1–4, 2015.
18. Kaur, G., M. Rattan, and C. Jain, "Optimization of swastika slotted fractal antenna using genetic algorithm and bat algorithm for S-band utilities," *Wireless Personal Communications*, Vol. 97, No. 1, 95–107, 2017.
19. Kaur, G., M. Rattan, and C. Jain, "Design and optimization of psi ( $\psi$ ) slotted fractal antenna using ANN and GA for multiband applications," *Wireless Personal Communications*, Vol. 97, No. 3, 4573–4585, 2017.
20. Choo, H. and H. Ling, "Design of multiband microstrip antennas using a genetic algorithm," *IEEE Microw. Wireless Compon. Lett.*, Vol. 12, No. 9, 345–347, 2002.
21. Jayasinghe, J. W., J. Anguera, and D. N. Uduwawala, "A simple design of multi band microstrip patch antennas robust to fabrication tolerances for GSM, UMTS, LTE, and Bluetooth applications by using genetic algorithm optimization," *Progress In Electromagnetics Research M*, Vol. 27, 255–269, 2012.
22. Martinez-Fernandez, J., J. M. Gil, and J. Zapata, "Ultrawideband optimized profile monopole antenna by means of simulated annealing algorithm and the finite element method," *IEEE Trans. Antennas Propag.*, Vol. 55, No. 6, 1826–1832, 2007.

23. Alaydrus, M. and T. F. Eibert, "Optimizing multiband antennas using simulated annealing," *2nd International ITG Conference on Antennas*, 86–90, 2007.
24. Dastranj, A., "Optimization of a printed UWB antenna: Application of the invasive weed optimization algorithm in antenna design," *IEEE Antennas and Propagation Magazine*, Vol. 59, No. 1, 48–57, 2017.
25. Monavar, F. M., N. Komjani, and P. Mousavi, "Application of invasive weed optimization to design a broadband patch antenna with symmetric radiation pattern," *IEEE Antennas Wireless Propag. Lett.*, Vol. 10, 1369–1372, 2011.
26. Karimkashi, S. and A. A. Kishk, "Invasive weed optimization and its features in electromagnetics," *IEEE Trans. Antennas Propag.*, Vol. 58, No. 4, 1269–1278, 2010.
27. Liu, W.-C., "Design of a multiband CPW-fed monopole antenna using a particle swarm optimization approach," *IEEE Trans. Antennas Propag.*, Vol. 53, No. 10, 3273–3279, October 2005.
28. Jin, N. and Y. Rahmat-Samii, "Parallel particle swarm optimization and finite-difference time-domain (PSO/FDTD) algorithm for multiband and wide-band patch antenna designs," *IEEE Trans. Antennas Propag.*, Vol. 53, No. 11, 3459–3468, 2005.
29. Jin, N. and Y. Rahmat-Samii, "Hybrid real-binary particle swarm optimization (HPSO) in engineering electromagnetics," *IEEE Trans. Antennas Propag.*, Vol. 58, No. 12, 3786–3794, 2010.
30. Jin, N. and Y. Rahmat-Samii, "Advances in particle swarm optimization for antenna designs: Real-number, binary, single-objective and multiobjective implementation," *IEEE Trans. Antennas Propag.*, Vol. 55, No. 3, 556–567, 2007.
31. Choudhury, B., S. Manickam, and R. M. Jha, "Particle swarm optimization for multiband metamaterial fractal antenna," *Journal of Optimization*, 2013.
32. Sun, L.-L., J.-T. Hu, K.-Y. Hu, M.-W. He, and H.-N. Chen, "Multi-species particle swarms optimization based on orthogonal learning and its application for optimal design of a butterfly-shaped patch antenna," *J. Cent. South Univ.*, Vol. 23, No. 8, 2048–2062, 2016.
33. Tang, M.-C., X. Chen, M. Li, and R. Ziolkowski, "Particle swarm optimized, 3D-printed, wideband, compact hemispherical antenna," *IEEE Antennas Wireless Propag. Lett.*, Vol. 17, No. 11, 2031–2035, 2018.
34. Chen, Y.-S., "Performance enhancement of multiband antennas through a two-stage optimization technique," *Int. J. RF Microw. Comput. Aided Eng.*, Vol. 27, No. 2, 1–9, 2016.
35. Bianchi, D., S. Genovesi, and A. Monorchio, "Constrained Pareto optimization of wide band and steerable concentric ring arrays," *IEEE Trans. Antennas Propag.*, Vol. 60, No. 7, 3195–3204, 2012.
36. Goudos, S. K., K. Siakavara, E. E. Vafiadis, and J. N. Sahalos, "Pareto optimal Yagi-Uda antenna design using multi-objective differential evolution," *Progress In Electromagnetics Research*, Vol. 105, 231–251, 2010.
37. Tuan, H. N., M. Hisashi, K. Yoshio, I. Kazuhiro, and N. Shinji, "A multi-level optimization method using PSO for the optimal design of an L-shaped folded monopole antenna array," *IEEE Trans. Antennas Propag.*, Vol. 62, No. 1, 206–215, 2014.
38. Balanis, C. A., *Antenna Theory: Analysis and Design*, 4th Edition, John Wiley & Sons, 2016.